

CHARACTERISTICS OF PLASMA ELECTROLYTIC OXIDATION COATINGS ON 6061 Al ALLOY PREPARED AT DIFFERENT CURRENT DENSITIES

Quang-Phu Tran^{1,*}, Van-Da Dao¹, Van-Hoi Pham²

¹Department of Electrical and Electronic Engineering, Hung Yen University of Technology and Education, 39A Road, Dan Tien Commune, Khoai Chau District, Hung Yen Province, Viet Nam

²Institute of Materials Science, Vietnam Academy of Science and Technology, 18 Hoang Quoc Viet Road, Cau Giay District, Ha Noi, Viet Nam

*Email: tranquangphu@utehy.edu.vn

Received: 11 May 2020; Accepted for publication: 10 November 2020

Abstract. Plasma electrolytic oxidation (PEO) has earned much attention due to its powerful and easy formation of hard and corrosion-resistant oxide layers on valve metals, such as Al alloys. Here we report the effects of current density (CD) on microstructure and properties of coatings on 6061 Al alloy by PEO using direct current mode. The electrolyte contains the chemicals of Na_2SiO_3 , $\text{Na}_2\text{WO}_4 \times 2\text{H}_2\text{O}$, and $\text{NaH}_2\text{PO}_2 \times \text{H}_2\text{O}$. The CDs adopted 5.0, 7.5, 10.0, and 12.5 A/dm^2 , respectively, for a fixed PEO time of 30 min. The thickness, surface morphology, phase composition, hardness, and corrosion resistance of PEO coatings as a function of the applied CD have been studied and discussed. Studied results show the coating thickness is proportional to the applied CD. When the applied CD increased 2.5 times from 5.0 to 12.5 A/dm^2 , the growth rate of oxide layers increased by more than 3.5 times, from 0.423 to 1.493 $\mu\text{m}/\text{min}$, respectively. SEM images are characterized by a reduction in the ratio of agglomerate-bumps-region/flatten-region as applied CD increases. However, cracks and larger pores appear when the applied CD is higher than 10.0 A/dm^2 . X-ray diffraction pattern shows that the main phases of Al, $\gamma\text{-Al}_2\text{O}_3$, $\alpha\text{-Al}_2\text{O}_3$, and W are contained in all coatings. PEO coated sample has the highest hardness of 1290 HV and highest polarization resistance of $8.80 \times 10^6 \Omega\text{cm}^2$ obtained at applied CD of 10 A/dm^2 which shows the best performance of the coating. The variation in coating performance is explained by microstructure details, specifically phases, compositions of oxide-layers, and micro-pores and cracks.

Keywords: plasma electrolytic oxidation (PEO), current density, 6061 Al alloy, micro-hardness, corrosion resistance.

Classification numbers: 2.5.2, 2.5.3, 2.9.1.

1. INTRODUCTION

Plasma electrolytic oxidation (PEO), also called micro-arc oxidation (MAO), is an atmospheric pressure surface treatment that provides excellent wear- and corrosion-resistant

coatings on valve metals such as Mg, Ti and their alloys, in particular on aluminium [1 - 6]. PEO is an application-specific surface-treatment technique extended from traditional anodizing via much higher applied voltages (200 ~ 600 V). PEO process contains alternation breakdown and formation of denser oxide layers which have excellent mechanical and electrochemical properties. Here emphasis is given to dielectric breakdown that initiates discharge events occurring on relatively weak dielectric area of the oxide layer. A much harder and denser structure was then formed via melting-and-quenching at the oxide-layer/substrate interfaces. Compared with traditional anodizing, PEO-formed oxide layers are 10 ~ 40 times thicker (up to 250 μm) with 5 ~ 8 times micro-hardness (up to 2535 HV) [7]. PEO coatings are much potential and extensively applicable for industry.

Formation of PEO coatings is sensitively influenced by different factors such as type of electrical power used (direct current, alternative current, pulsed currents, etc.), type of substrate, electric field distribution, electrolyte characteristics (composition, pH, conductivity and temperature), behavior of discharge and also duration of treatment [8], which require detail investigation.

Electrical power supply is of particular concern not only due to its influence on the quality of oxide layers, but also relating to the cost of PEO equipment and coating process. The factors relating to the electric sources include type of electric source, voltage, current density (CD) and pulse parameters (frequency of current, duty cycle). All these factors have been mentioned in the literatures. These factors of electric source can affect the surface discharge characteristics such as the intensity and density of discharge and hence affect the features of coating such as size and distribution of pore, thickness, roughness, etc. [9]. Types of electric source for PEO process are mainly direct current (DC) [10 - 13], pulsed-DC [14 - 17] or pulsed-bipolar current [18 - 21]. Pulsed-DC and pulsed-bipolar current are increasingly used although they have a very high cost. Due to the simple and inexpensive, constant DC power is still used since discovering the PEO technique to present. Voltage and current density are important parameters affecting the PEO coating properties. PEO process can be controlled with the constant voltage [19, 22, 23] or constant current density [24 - 27]. When PEO process is kept at constant voltage, the current density will be reducing with the treatment time. When PEO process is kept at constant current density, the voltage will be increasing with the treatment time. These are due to the gradual thickening of ceramic layer formed [6]. Khan *et al.* prepared MAO coatings on 6082 Al alloy using constant DC power supply with various current density ranging from 5 A/dm^2 to 20 A/dm^2 . Their results indicated that higher current density leads to thicker coating film with minimal stress level, dense surface morphology and increased $\alpha\text{-Al}_2\text{O}_3$ content [28]. Raj *et al.* reported that the thickness and growth rate of MAO coating increase with increasing direct current densities (5 - 15 A/dm^2). But when current density is higher than a certain value (20 A/dm^2) properties of coating are deteriorated due to the dissolution of the coating over the coating formation [29]. They also reported that the thickness and growth rate of the coating increases with increasing applied voltage.

In this study, we used DC mode as a power source of PEO process and investigated the effects of current density on microstructure and properties of coatings on 6061 Al alloy, where the electrolytes containing sodium silicate, sodium tungstate dehydrate and sodium hypophosphite monohydrate are used. We investigated the effects of concentration of each chemical composition (sodium silicate, sodium tungstate dehydrate and sodium hypophosphite monohydrate) in the electrolyte on properties of PEO coated 6061 Al alloy in other work (not showed in this study), and the optimal electrolyte which shows the best performance of coatings is selected for present study. We focused on the effects of CD upon coating characteristics;

specifically formed crystalline phases, composition in phases, micro-hardness, and corrosion resistance.

2. MATERIALS AND METHODS

Rectangular samples of 6061 aluminium alloy (0.15 ~ 0.4 % Cu, 0.15 % Mn, 0.8 ~ 1.2 % Mg, 0.25 % Zn, 0.04 ~ 0.35 Cr, 0.15% Ti, 0.4 ~ 0.8 % Si, 0.7 % Fe, and balanced aluminium) with size 20 × 20 × 3 mm were ground by abrasive papers up to #2000, to achieve a surface roughness $R_a \approx 0.1 \mu\text{m}$. Before the start of each experiment, the samples were cleaned via ultrasonic cleaning using acetone, ethanol and deionized water to removes grease. A two liter stainless steel tank was filled with electrolytes contained Na_2SiO_3 (4 g/L), $\text{Na}_2\text{WO}_4 \times 2\text{H}_2\text{O}$ (6 g/L) and $\text{NaH}_2\text{PO}_2 \times \text{H}_2\text{O}$ (4 g/L). An aluminium wire was spot-welded to the sample to ensure the current transfer during the PEO process. The sample was immersed into electrolyte. The aluminium wire was connected to anode side of a DC power supply (KYOSAN), while the stainless steel tank was connected to cathode side. Stainless steel tank was

placed into a glass tank of cold water which keeps the bath temperature below 40 °C. The water is cooled thanks to a stainless steel coil with cooling water inside that has been soaked in the water tank. Various constant current densities of 5.0, 7.5, 10.0 and 12.5 A/dm², respectively, were set and maintained during 30 min PEO processing. The schematic diagram of the PEO system is shown in Fig. 1.

After the PEO treatments, an eddy current type coating thickness tester (Kett LZ-373) provides a non-destructive method for measurement of coating thickness. For each PEO coating, twenty measurements were taken in center regime (to avoid boundary effects) to evaluate the average coating thickness with a standard deviation ($\pm 0.1 \mu\text{m}$). An X-ray diffractometer (XRD, Bruker D8 Discover) using $\text{Cu } k_{\alpha 1}$ radiation was employed to analyse crystalline phases in PEO coatings. Each sample was scanned from 10° to 80° with a scanning rate of 4° min⁻¹. Surface morphology was studied via a scanning electron microscope (SEM, HITACHI-S3400). The accessory EDX analysis of the SEM was used to analyse the distribution of chemical elements across the coating thickness. To analyse mechanical properties, we used a micro-hardness tester (FM-300e) to measure micro-hardness of the coating. The measurements were carried out with 25 g loading on 10 random locations of each coating to evaluate an average result. A CHI Electrochemical Analyser was employed to study the properties of corrosion resistance with a three-electrode cell system in 3.5 wt% NaCl solution at room temperature, in which a saturated calomel electrode (SCE), a platinum grid, and the sample are acting as reference electrode, counter electrode, and working electrode, respectively. All the samples were immersed in the electrolyte until stabilize, and then analysed of the open circuit potential for 100 second before

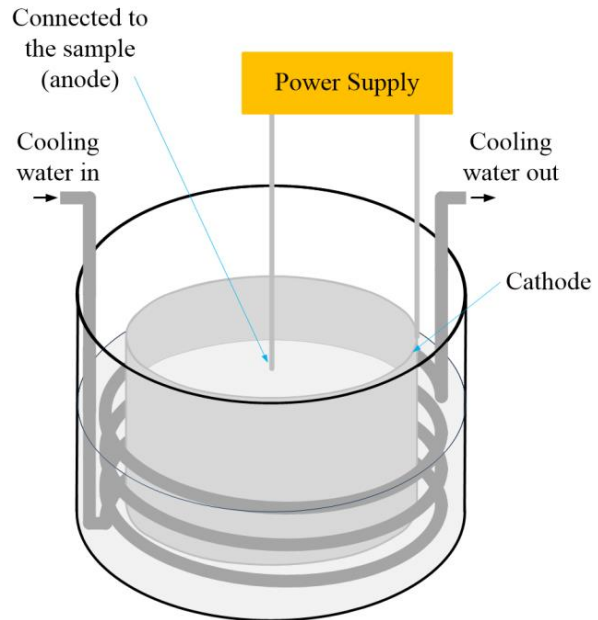


Figure 1. Schematic diagram of the PEO system.

the potential-dynamic analysis. The parameters of potential-dynamic analysis were executed with a scanning range from -2 V to 2 V (vs. open circuit potential) at a scanning rate 0.01 V/s on a 1 cm² area.

3. RESULTS AND DISCUSSION

3.1. Voltage–time responses and coating thickness with difference of applied CDs

Figure 2 represents the voltage transient recorded during the PEO treatment with various current densities from 5 to 12.5 A/dm². Three different PEO stages are identifiable according to the slope of voltage transient. They are Faraday region, Spark discharge region and Micro-arc Oxidation region. In the Faraday region, substrate is immediately passivated based on the Faraday's law, in which the voltage increases linearly with time. The rise of electric field strength causes dielectric breakdown on the strong passive layer. In the second region, the voltage increase rate is rather low due to the concurrent occurrence of oxidation and dissolution. After reaching the onset of sparking, electrical sparks occur with gas evolution. In the Micro-arc oxidation region, the voltage increases even slower indicating a sluggish coating formation rate [30].

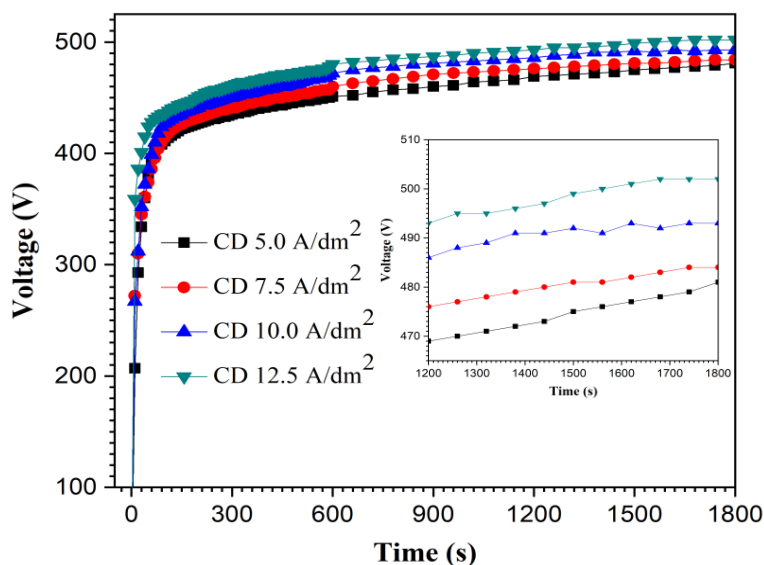


Figure 2. Voltage transients during PEO processing under various applied current densities ($5 \sim 12.5$ A/dm²).

The response voltages after PEO process for 30 minutes were of 481 , 484 , 493 and 502 volts versus current densities of 5.0 , 7.5 , 10.0 , and 12.5 A/dm², respectively (see the inset image in Figure 2). The recorded of response voltages are also collected in Table 1. It indicated that the applied current density is also a factor influencing the final voltage. When higher current density is applied for PEO treatment, higher voltage responses due to higher oxide layer formation rate which follows Ohmic's law [30].

The average coating thickness of PEO coatings is continuously increasing with increasing applied CD. As shown in Table 1, the average coating thickness is 12.7 μm , 16.4 μm , 33.4 μm , and 44.8 μm when applied CD as 5 A/dm², 7.5 A/dm², 10 A/dm², and 12.5 A/dm², respectively. This indicated the growth rate of coating thickness from 0.423 $\mu\text{m}/\text{min}$ to 1.493 $\mu\text{m}/\text{min}$ as applied CD increased from 5 A/dm² to 12.5 A/dm², respectively.

Table 1. PEO coating characteristics under the different applied current densities.

PEO Current Density (A/dm ²)	blank	5.0	7.5	10.0	12.5
Respond voltage after 30 min. (V)	-	481	484	493	502
Thickness (μm)	-	12.7 ± 1.5	16.4 ± 3.3	33.4 ± 5.1	44.8 ± 8.2
Growth rate (μm/min)	-	0.423	0.547	1.113	1.493
Micro-Hardness (HV)	60	1211 ± 47	1247 ± 36	1290 ± 32	1248 ± 66

3.2. Effects of current density on structure and hardness of the PEO layers

Figure 3 shows surface morphology of Al-PEO coatings fabricated by different CDs. The images indicate that the ratio of agglomerate-bumps-region/flatten-region is higher with lower applied CD. This phenomenon is due to incomplete process occurring under lower applied energy. However, cracking occurs on coating surface under 12.5 A/dm² applied CD due to the thermal stress. On the other hand, the relatively large pores with less porosity only occur at the condition of 12.5 A/dm².

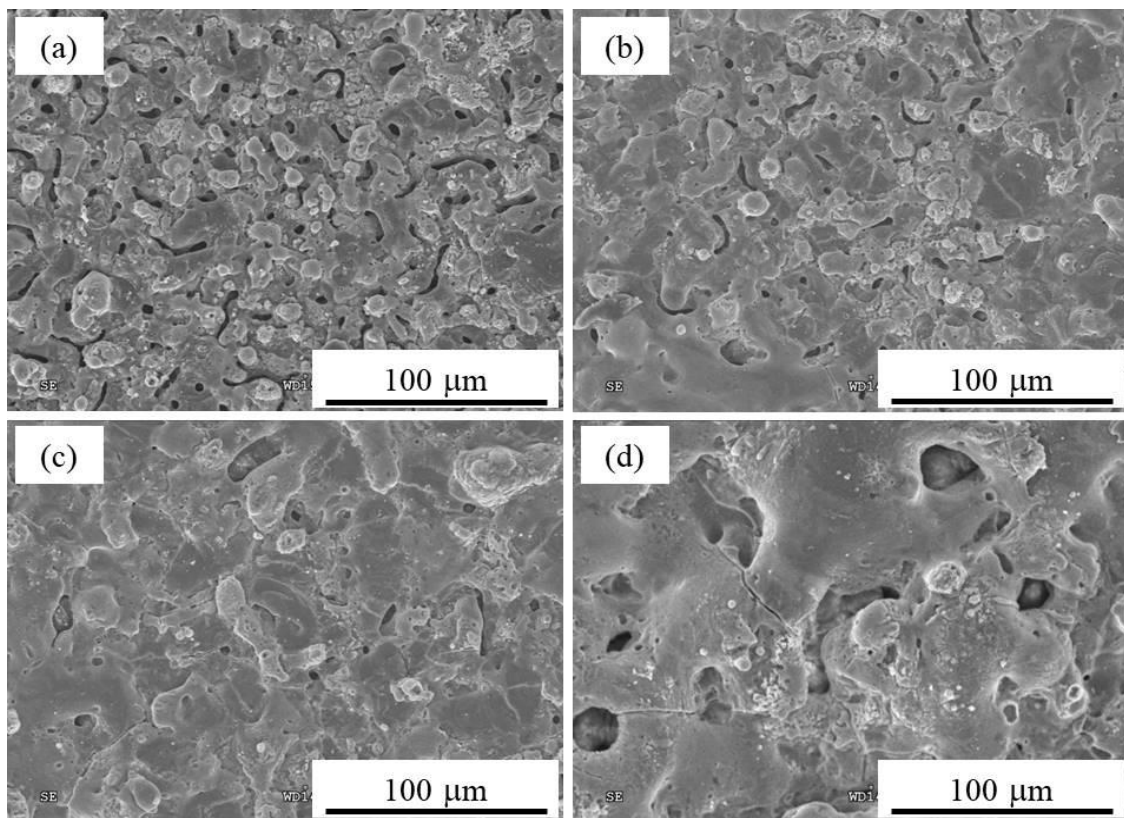


Figure 3. SEM images of surface morphology on PEO coating of 6061 Al-alloy under current density of (a) 5.0 A/dm², (b) 7.5 A/dm², (c) 10.0 A/dm² and (d) 12.5 A/dm².

XRD patterns of Al-PEO coatings under various current densities are shown in Figure 4. The XRD patterns indicate the main phases of Al (JCPDS card No. 04-0787), γ - Al_2O_3 (JCPDS card No. 10-0425), W (JCPDS card No. 04-0608), and α - Al_2O_3 (JCPDS card No. 10-0173). α - Al_2O_3 phase can be slightly identified when increasing CD, in which the input energy is high enough to cause recrystallization [2], however, the signal of α - Al_2O_3 pattern was still feeble even under the 12.5 A/dm^2 condition of this study. The intensity of metallic W phase increases obviously with increasing CD. With more α - Al_2O_3 and metallic W phase present, ideally the coating hardness should also be improved. However, as shown in

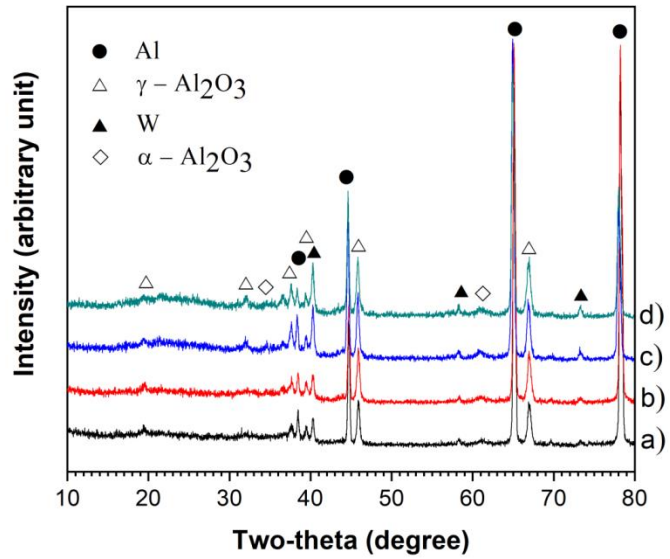


Figure 4. XRD patterns of PEO coatings on 6061 Al-alloy under various current densities: a) 5.0 A/dm^2 , b) 7.5 A/dm^2 , c) 10.0 A/dm^2 , and d) 12.5 A/dm^2 .

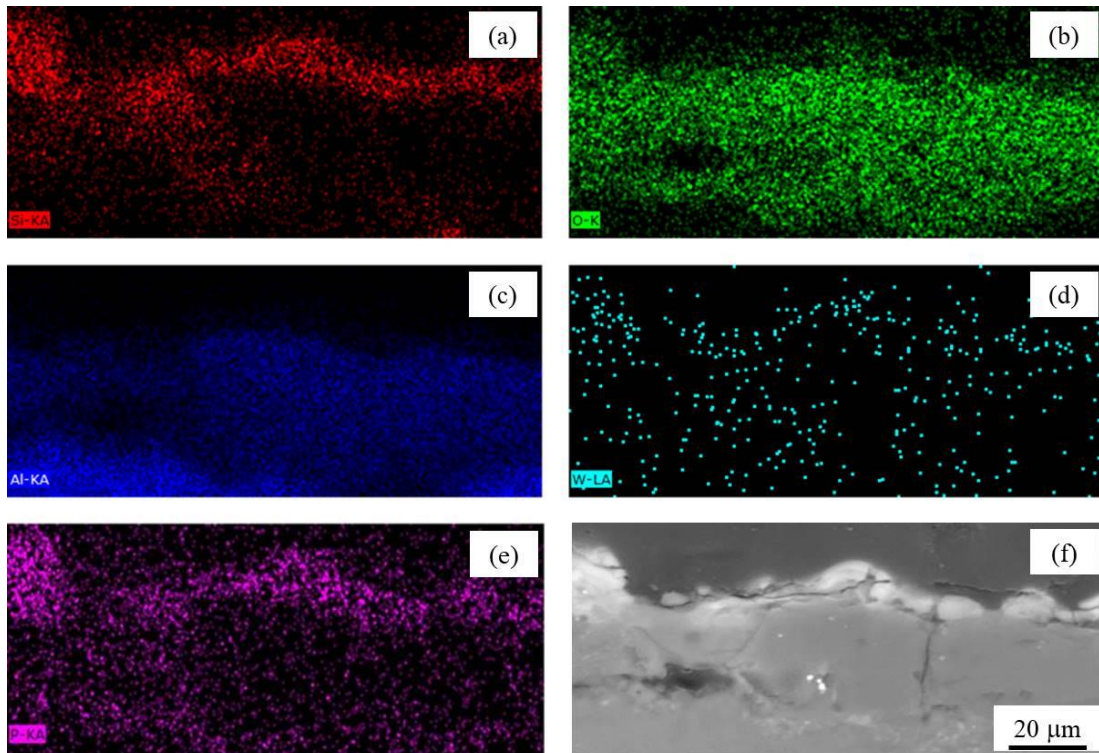


Figure 5. Cross-sectional SEM image with elements mapping of PEO layer at applied current density of 10 A/dm^2 : (a) Si; (b) O; (c) Al; (d) W; (e) P elements; and (f) SEM micrograph image.

Table 1, the coating with the highest hardness of 1290 HV is fabricated by using $CD = 10 \text{ A/dm}^2$. It can be explained by the cracking found on the coatings and the effect of tiny $\alpha\text{-Al}_2\text{O}_3$ phase containing is negligible. As CD is higher than 10 A/dm^2 , stronger thermal stresses will occur due to more energy input, larger coating thickness and/or the layer-formation rate.

The SEM cross-sectional images with EDX mapping of Si, Al, P, O, and W elements on PEO coating at applied CD 10.0 A/dm^2 were shown in Figure 5. It is seen that the Al and O elements are distributed homogeneously in the coating. The distribution of Si and P gathered on the top region of the PEO layer. However, the component of tungsten was scarce to represent the trend of distribution.

3.3. Corrosion behaviors of the PEO coatings obtained by different current densities

Figure 6 represents polarization curves of the bare and PEO coated 6061 Al alloy produced under various applied CDs. The extracted parameters of corrosion potential E_{corr} , corrosion current density I_{corr} , cathodic and anodic Tafel slopes (β_c and β_a) are collected in Table 2. The polarization resistance values R_p (in Ωcm^2) were calculated by using Stern-Geary equation [31]

$$R_p = \frac{\beta_c \times \beta_a}{2.302 I_{corr} (\beta_c + \beta_a)} \quad (1)$$

and also collected in Table 2.

In comparison with the bare 6061 Al alloy, all the PEO coated samples show a decreasing in corrosion current density and an increasing in corrosion resistance by at least two orders of magnitude, with a large positive shift of the corrosion potential. Corrosion current density of the PEO sample with CD of 5.0 A/dm^2 is $7.93 \times 10^{-7} \text{ A/cm}^2$ which decreases to $1.28 \times 10^{-7} \text{ A/cm}^2$ and reaches the smallest value of $7.45 \times 10^{-8} \text{ A/cm}^2$ when the applied CD is 7.5 A/dm^2 and 10.0 A/dm^2 , respectively. The higher applied CD (12.5 A/cm^2) leads to an increase of corrosion current density ($2.22 \times 10^{-7} \text{ A/cm}^2$). It can also be seen the polarization resistance is increased with the

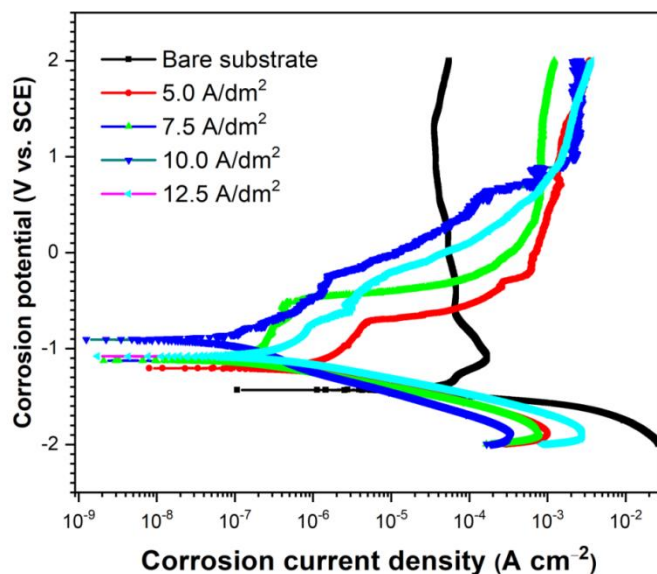


Figure 6. Polarization curves of PEO coatings on 6061 Al-alloy processed with the different current densities.

increase of the applied CD and reaches the highest value of $8.80 \times 10^6 \Omega\text{cm}^2$ as the applied CD is 10.0 A/dm^2 . So, the coating with the best corrosion resistance is under the conditions of applied CD 10.0 A/dm^2 , in which the corrosion current density I_{corr} is 34 times smaller and the polarization resistance is 418 times higher than those of the bare 6061 Al. The corrosion resistance is affected by key factors such as thickness, porosity, coherence [32]. The reduction of pores and increase of coating thickness with increase the applied CD $5.0 \sim 10.0 \text{ A/dm}^2$ are the reasons of improvement in corrosion resistance. While the appearance of large pores and cracks

at the applied CD 12.5 A/dm² deteriorate corrosion resistance despite higher coating thickness.

Table 2. Electrochemical parameters extracted from potentiodynamic polarization curves of bare 6061 Al-alloy and PEO samples with the different applied current densities.

PEO Current Density (A/dm ²)	blank	5.0	7.5	10.0	12.5
E _{corr} (V)	-1.433	-1.207	-1.122	-0.909	-1.082
I _{corr} (A/cm ²)	3.24 × 10 ⁻⁵	7.93 × 10 ⁻⁷	1.28 × 10 ⁻⁷	7.45 × 10 ⁻⁸	2.22 × 10 ⁻⁷
β _c (V)	15.105	7.736	7.946	5.488	8.178
β _a (V)	1.752	3.695	2.861	2.084	3.735
R _p (Ωcm ²)	2.11 × 10 ⁴	1.37 × 10 ⁶	7.14 × 10 ⁶	8.80 × 10 ⁶	5.01 × 10 ⁶

4. CONCLUSIONS

In this study, the influence of applied current density was investigated on the layer formation and performance of PEO coating on 6061 Al alloy using a DC mode. The results indicate that the applied CD much affects to the characteristics of PEO coatings. The coating thickness increased from 12.7 μm to 44.8 μm as the applied CD increased from 5 A/dm² to 12.5 A/dm² which showed the corresponding growth rate from 0.423 μm/min to 1.493 μm/min, respectively. Surface morphology is characteristic of reducing the number of bulges and increasing flattened regions on the coating surface with the increasing of the applied CD, however, cracks and large pores appeared on coating surface at the applied CD of 12.5 A/dm². XRD analysis results indicate the main phases are Al, γ-Al₂O₃, W, and α-Al₂O₃. The peak intensity of W and α-Al₂O₃ phases are slightly increased with increasing applied CD. Hardness and corrosion resistance of PEO coatings are increased with the increasing of applied CD from 5 A/dm² to 10 A/dm² which shows the highest value of hardness and polarization resistance of 1290 HV and 8.80 × 10⁶ Ωcm², respectively. The higher applied CD causes a decrease in hardness and corrosion resistance due to the appearance of large pores and cracks. The integration results indicate that, no matter what the coating thickness is, formation rate, the size of surface pores, the occurrence of cracks all impact both mechanical and electrochemical properties of the PEO coatings.

Acknowledgments: This research is funded by Vietnam National Foundation for Science and Technology Development (NAFOSTED) under grant number 103.99-2017.69, and by Hung Yen University of Technology and Education under grand number UTEHY.L.2020.33.

REFERENCES

1. Voevodin A., Yerokhin A., Lyubimov V., Donley M., Zabinski J. - Characterization of wear protective Al₂O₃SiO₂ coatings formed on Al-based alloys by micro-arc discharge treatment, *Surface and Coatings Technology* **86** (1996) 516-521.
2. Yerokhin A. L., Nie X., Leyland A., Matthews A., Dowey S. J. - Plasma electrolysis for surface engineering, *Surface and Coatings Technology* **122** (1999) 73-93.
3. Tran Q. P., Sun J. K., Kuo Y. C., Tseng C. Y., He J. L., Chin T. S. - Anomalous layer-thickening during micro-arc oxidation of 6061 Al alloy, *Journal of Alloys and Compounds* **697** (2017) 326-332.

4. Tran Q. P., Chin T. S., Kuo Y. C., Jin C. X., Trung T., Van Tuan C., Dang D. Q. - Diamond powder incorporated oxide layers formed on 6061 Al alloy by plasma electrolytic oxidation, *Journal of Alloys and Compounds* **751** (2018) 289-298.
5. Tran Q. P., Chin T. S. - Plasma electrolytic oxidation coating on 6061 Al alloy using an electrolyte without alkali ions, *Vietnam Journal of Science and Technology* **54** (5A) (2016) 151-158.
6. Tran Q. P., Kuo Y. C., Sun J. K., He J. L., Chin T. S. - High quality oxide-layers on Al-alloy by micro-arc oxidation using hybrid voltages, *Surface and Coatings Technology, Part A* **303** (2016) 61-67.
7. Wu H., Wang J., Long B., Long B., Jin Z., Naidan W., Yu F., Bi D. - Ultra-hard ceramic coatings fabricated through microarc oxidation on aluminium alloy, *Applied surface science* **252** (2005) 1545-1552.
8. Yang G. L., Lü X. Y., Bai Y. Z., Cui H. F., Jin Z. S. - The effects of current density on the phase composition and microstructure properties of micro-arc oxidation coating, *Journal of Alloys and Compounds* **345** (2002) 196-200.
9. Hussein R. O., Northwood D. O., Su J. F., Nie X. - A study of the interactive effects of hybrid current modes on the tribological properties of a PEO (plasma electrolytic oxidation) coated AM60B Mg-alloy, *Surface and Coatings Technology* **215** (2013) 421–430.
10. Wang L., Fua W., Chen L. - Evolution of active species and discharge sparks in Na₂SiO₃ electrolyte during PEO process, *Journal of Alloys and Compounds* **509** (2011) 7652–7656.
11. Javidi M., Fadaee H. - Plasma electrolytic oxidation of 2024-T3 aluminum alloy and investigation on microstructure and wear behavior, *Applied Surface Science* **286** (2013) 212-219.
12. Khan R. H. U., Yerokhin A. L., Pilkington T., Leyland A., Matthews A. - Residual stresses in plasma electrolytic oxidation coatings on Al alloy produced by pulsed unipolar current, *Surface and Coatings Technology* **200** (2005) 1580-1586.
13. Wang L., Nie X. - Silicon effects on formation of EPO oxide coatings on aluminum alloys, *Thin Solid Films* **494** (2006) 211-218.
14. Han I., Choi J. H., Zhao B. H., Baik H. K., Lee I. S. - Changes in anodized titanium surface morphology by virtue of different unipolar DC pulse waveform, *Surface and Coatings Technology* **201** (2007) 5533-5536.
15. Lv G., Gu W., Chen H., Feng W., Khosa M. L., Li L., Niu E., Zhang G., Yang S. Z. - Characteristic of ceramic coatings on aluminum by plasma electrolytic oxidation in silicate and phosphate electrolyte, *Applied Surface Science* **253** (2006) 2947-2952.
16. Gao H. T., Zhang M., Yang X., Huang P., Xua K. - Effect of Na₂SiO₃ solution concentration of micro-arc oxidation process on lap-shear strength of adhesive-bonded magnesium alloys, *Applied Surface Science* **314** (2014) 447-452.
17. Liu X. H., Zhu L. Q., Liu H. C., Li W. P. - Investigation of MAO coating growth mechanism on aluminum alloy by two-step oxidation method, *Applied Surface Science* **29** (2014) 12-17.
18. Nie X., Meletis E. I., Jiang J. C., Leyland A., Yerokhin A. L., Matthews A. - Abrasive wear/corrosion properties and TEM analysis of Al₂O₃ coatings fabricated using plasma electrolysis, *Surface and Coatings Technology* **149** (2002) 245-251.

19. Yazıcı S. K., Muhaffel F., Baydogan M. - Effect of incorporating carbon nanotubes into electrolyte on surfacemorphology of micro arc oxidized Cp-Ti, *Applied Surface Science* **318** (2014) 10-14.
20. Wang J. H., D M. H., Han F. Z., Yang J. - Effects of the ratio of anodic and cathodic currents on the characteristics of micro-arc oxidation ceramic coatings on Al alloys, *Applied Surface Science* **292** (2014) 658-664.
21. Shen D. J., Li G. L., Guo C. H., Zou J., Cai J. R., He D. L., Ma H. J., Liu F. F. - Microstructure and corrosion behavior of micro-arc oxidation coating on 6061 aluminum alloy pre-treated by high-temperature oxidation, *Applied Surface Science* **287** (2013) 451-456.
22. Long B. H., Wu H. H., Long B. Y., Wang J. B., Wang N. D., Lu X. Y., Jin Z. S., Bai Y. Z. - Characteristics of electric parameters in aluminium alloy MAO coating process, *Journal of Physics D: Applied Physics* **38** (2005) 3491-3496.
23. Khaselev O., Yahalom J. - The anodic behaviour of binary Mg-Al alloys in KOH aluminate solutions, *Corrosion Science* **40** (1998) 1149-1160.
24. Gu W. C., Lv G. H., Chen H., Chen G. L., Feng W. R., Yang S. Z. - Characterisation of ceramic coatings produced by plasma electrolytic oxidation of aluminum alloy, *Materials Science and Engineering A* **447** (2007) 158-162.
25. Wasekar N. P., Jyothirmayi A., Sundararajan G. - Influence of prior corrosion on the high cycle fatigue behavior of microarc oxidation coated 6061-T6 aluminum alloy, *International Journal of Fatigue* **33** (2011) 1268-1276.
26. Jin F. Y., Chu P. K., Tong H. H., Zhao J. - Improvement of surface porosity and properties of alumina films by incorporation of Fe micrograins in micro-arc oxidation, *Applied Surface Science* **253** (2006) 863-868.
27. Kaseem M., Kamil M. P., Kwon J. H., Ko Y. G. - Effect of sodium benzoate on corrosion behavior of 6061 Al alloy processed by plasma electrolytic oxidation, *Surface and Coatings Technology* **283** (2015) 268-273.
28. Khan R. H. U., Yerokhin A., Li X., Dong H., Matthews A. - Surface characterization of DC plasma electrolytic oxidation treated 6082 aluminium alloy: effect of current density and electrolyte concentration, *Surface and Coating Technology* **205** (2010) 1679-1688.
29. Raj V., Ali M. M. - Formation of ceramic alumina nanocomposite coatings on aluminium for enhanced corrosion resistance, *Journal of Materials Processing Technology* **209** (2009) 5341-5352.
30. Snizhko L., Yerokhin A., Pilkington A., Gurevina N., Misnyankin D., Leyland A., Matthews A. - Anodic processes in plasma electrolytic oxidation of aluminium in alkaline solutions, *Electrochimica Acta* **49** (2004) 2085-2095.
31. Stern M., Geary A. L. J. J. - Electrochemical polarization I. A theoretical analysis of the shape of polarization curves, **104** (1957) 56-63.
32. Sarbishei S., Faghihi Sani M. A., Mohammadi M. R. - Study plasma electrolytic oxidation process and characterization of coatings formed in an alumina nanoparticle suspension, *Vacuum* **108** (2014) 12-19.